Electrochimica Acta 209 (2016) 121–131

Contents lists available at ScienceDirect

Electrochimica Acta

journal homepage: www.elsevier.com/locate/electacta

Mechanism of ethanol electrooxidation on mesoporous Pt electrode in acidic medium studied by a novel electrochemical mass spectrometry set-up

Jonathan Flórez-Montaño[a], Gonzalo García[a,*], Olmedo Guillén-Villafuerte[a], José Luis Rodríguez[a], Gabriel A. Planes[b], Elena Pastor[a,*]

[a] Instituto de Materiales y Nanotecnología, Universidad de La Laguna, Avda. Astrofísico Francisco Sánchez s/n, 38071 La Laguna, Santa Cruz de Tenerife, Spain
[b] Universidad Nacional de Río Cuarto, Ruta Nac. 36, Km 601, Río Cuarto, Córdoba, Argentina

ARTICLE INFO

Article history:
Received 22 October 2015
Received in revised form 6 May 2016
Accepted 9 May 2016
Available online 10 May 2016

Keywords:
Ethanol electrooxidation
Mesoporous platinum
EC-MS
Carbon dioxide
Fuel cells

ABSTRACT

The electrochemical behavior and mass spectrometric features for ethanol reactions on nanostructured mesoporous platinum catalysts (MPPt) in 0.5 M H_2SO_4 were studied for the first time as function of the alcohol concentration. With this purpose, cyclic voltammetry and chronoamperometry techniques were combined with a new configuration of an electrochemical mass spectrometry (EC-MS), which allows high detection sensitivity with low amount of catalysts. Accordingly, a comprehensive study of the reaction mechanism and kinetics of the ethanol oxidation on MPPt in acidic medium was carried out. The water dissociation reaction and the first ethanol dehydrogenation step are proposed to be the rate-determining step (*rds*) for the complete ethanol oxidation reaction and the acetaldehyde production, respectively. Furthermore, acetaldehyde, acetic acid and CO_2 formation were monitored during the ethanol electrooxidation reaction and the energy conversion efficiency from ethanol to CO_2 was calculated. Results indicate an increment of by-side products (acetaldehyde and acetic acid) maintaining equal CO_2 formation with the rise of the alcohol concentration. Consequently, the highest energy conversion efficiency to CO_2 (~11%) was achieved at 0.6 V with the lowest alcohol concentration employed (0.01 M). Results were analyzed in terms of density and type of active surface sites, applied potential and alcohol concentration.

1. Introduction

Direct alcohol fuel cells (DAFCs) have attracted considerable interest in recent years because of their potential for portable applications. The main advantage of alcohols as fuel compared to hydrogen is that they are liquid, and therefore, the storage problems are solved. Additionally, the power density of alcohols in terms of energy per volume of fuel is much higher than hydrogen at standard conditions. Since ethanol is the major renewable bio-fuel and less toxic than other alcohols, it appears as a promising liquid fuel for DAFC systems [1–3].

Conventional fuel cell catalysts are mainly composed of metallic nanoparticles (e.g. Pt or Pt alloys) supported on high surface area carbon (e.g. carbon black). The properties of these materials, such as surface area and conductivity, determine the yield of the different electrochemical reactions taking place in DAFCs [4,5], although one of the main drawbacks is the facile catalyst support corrosion under the hard operating conditions. Contrary to conventional catalysts employed in these devices, non-carbon supported mesoporous (MP) metallic nanostructures are easily produced directly onto a conductive material, and therefore compact catalysts with high performance (high catalytic activity and high tolerance toward the corrosion) can be integrated in electronic devices such as micro fuel cells (μFC) and/or direct alcohol micro fuel cells (DAμFC).

Metallic MP catalysts can be synthesized by chemical or electrochemical reduction of metallic salts dissolved in the aqueous domains of a liquid crystal solution [6,7]. Usually, this simple process renders thin and shiny electrodes with high surface area and activity [7]. The MP structure, determined by the porous dimension and porosity degree, is easily tuned by adjusting the synthesis parameters, such as the surfactant, reduction potential and time expended at the applied potential [8]. Usually, the

* Corresponding authors. Tel.:+ 34 922 318071; fax: +34 922 318002.
E-mail addresses: ggarcia@ull.edu.es, gonau111@gmail.com (G. García), epastor@ull.edu.es (E. Pastor).

http://dx.doi.org/10.1016/j.electacta.2016.05.070
0013-4686/

catalysts synthesized contain a porous architecture with an extremely concave MP surface, which strongly affect the CO electrooxidation reaction [9] and improve the catalytic oxidation of the alcohols [10–13].

The full oxidation of ethanol to carbon dioxide has a favorable thermodynamic potential of 0.08 V (vs. RHE), although the efficiency of direct ethanol fuel cells is drastically limited by the formation of partial oxidation products (maintaining intact the carbon-carbon bond, such as acetaldehyde and acetic acid) and strongly adsorbed intermediates [14]. It is accepted that two main paths exist in the overall mechanism of ethanol oxidation at Pt-based electrodes [15]. The first involves the dissociative adsorption of ethanol to produce adsorbed species (CO and CH_x) at low potentials [16,17], whereas the second includes the formation of an adsorbed acetyl species (CH_3CO) that can be further oxidized to acetaldehyde and in presence of adsorbed OH to acetic acid and as a minor extent to carbon dioxide [18].

Pt-based catalysts such as PtSn [19] or PtRu [20] were suggested to enhance the electrocatalytic performance for ethanol electro-oxidation with respect to monometallic Pt catalyst. In this sense, it is believed that the use of oxophilic atoms increases the CO tolerance as they enhance the activation of water to form surface hydroxides, which are necessary to oxidize CO and possibly CH_x intermediates by the bifunctional mechanism or electronic effects [21]. In this context, not only foreign elements such as Ru or Sn (i.e. changes in the nature of the material) may produce oxygenated species at low overpotentials, but also Pt atoms located at special sites such as low-coordinated sites are known to easily dissociate water (i.e. effect of the surface geometric structure) [21]. Thus, mesoporous platinum (MPPt) catalysts with extremely high concave structure are expected to produce a synergetic effect during the CO and ethanol oxidation reactions.

The reactivity of ethanol on noble metal electrodes has been the subject of many spectroscopic investigations during the past years. Main identified products by in-situ Fourier transform infrared spectroscopy (FTIRS) [22–24] and on-line differential electrochemical mass spectrometry (DEMS) [25–27] during the ethanol oxidation on Pt in acidic solution were acetaldehyde, acetic acid, adsorbed carbon monoxide and CO_2. DEMS technique has proven to be a useful tool for the study of electrocatalytic processes, in which volatile or gaseous species are involved [10–14,25–31]. In this sense, it appears as an adequate technique to study the reaction mechanisms and the conversion efficiency to final products of the fuel employed in the fuel cell system. Quantitative and qualitative detection of reaction products and intermediates, as well as, the consumption of electroactive species can be easily followed. DEMS experiments showed low CO_2 conversion efficiencies from the ethanol oxidation on carbon-supported Pt catalysts (<3%) and smooth polycrystalline Pt surfaces (<2%) [14,26,27,29]. The efficiency of ethanol conversion to CO_2 depends on several factors such as an adequate DEMS set-up [30], the catalytic surface structure and nature [29–31], the alcohol concentration [32] and the working temperature [33]. Nevertheless, there is a consensus that the ethanol electrooxidation reaction is not complete and that acetaldehyde and acetic acid are the main responsible for the ca. 30 and 60% of the delivered faradaic current, respectively [27].

In the current work, ethanol electrooxidation in acidic medium is studied on MPPt catalyst for the first time by a new electrochemical mass spectrometry (EC-MS) configuration. This new set-up allows the use of massive electrodes as well as powder catalysts achieving high sensitivities with low amounts of material, being more versatile than other conventional electrochemical mass spectrometry designs. Reaction intermediates as well as ethanol oxidation products were detected, and the efficiency for ethanol oxidation to CO_2 was achieved for diverse ethanol concentrations.

2. Experiment measurement

2.1. Working electrode preparation.

MPPt electrodes were obtained by electrochemical reduction of a mixture of aqueous hexachloroplatinic acid (8%) and octa-ethylene glycol monohexadecyl ether ($C_{16}EO_8$) (50% weight fraction) onto an Au disk electrode (Ø = 2.5 mm) at 60 °C and 0.15 V as have been reported in early publications [9–12]. The complete physicochemical characterization has been also reported in these works. Briefly, a charge of 749 mC cm^{-2} was passed during the deposition onto the Au substrate, resulting in a mesoporous Pt layer containing 74.37 μg of Pt (assuming 75% efficiency). Then, the electrode was left in distilled water for 48 h replacing the liquid every 2 h. After that, the surface looks as a smooth and shining metallic Pt layer at the macroscopic level. Meanwhile, small grooves produced by the liquid crystal patterning are observed in the nanoscopic scale [10,11].

2.2. Electrochemical measurements

A thermostated three electrodes electrochemical cell was used to perform the analysis at 25 °C. This cell allows solution exchange under working electrode potential control. A carbon rod was used as counter electrode and a reversible hydrogen electrode (RHE) in the electrolyte as reference electrode. All potentials in this work are given against the RHE. Electrochemical measurements were performed with a PC Autolab potentiostat-galvanostat PGSTAT30.

Experiments were carried out in 0.5 M aqueous sulphuric solutions prepared from high purity reagents (Merck p.a.) and ultra-pure water (Millipore MilliQ gradient A10 system, 18.2 MΩ cm, 2 ppb total organic carbon). Argon (N50) was used to deoxygenate all solutions and CO (N47) to dose CO. CO stripping experiments were obtained after bubbling CO through the cell for 15 min while keeping the MPPt electrode at 0.20 V, followed by argon purging and electrolyte exchange to remove the excess of CO. CO stripping voltammograms were recorded, by first scanning negatively until 0.05 V so that entire hydrogen region was explored, and then scanning positively up to 1.0 V.

The charge involved in the CO oxidation peak was used to determine the electroactive surface area (ESA: 2.91 cm^2), assuming a charge of 388 μC cm^{-2} involved in the oxidation of 0.93 monolayer of linearly adsorbed CO. Current densities J given in the present paper were calculated with the previously achieved ESA.

Potentiodynamic and potentiostatic experiences of ethanol oxidation were performed with several alcohol concentrations (in the range from 0.01 to 1 M). First the working electrode was fixed to 0.05 V and later the alcohol solution was introduced into the electrochemical cell. Next, cyclic voltammograms (CVs) or current transients (CTs) were obtained by sweeping/stepping the potential from 0.05 V to the final oxidation potential.

2.3. EC-MS set-up

Gaseous species produced on the electroactive surface were continuously detected by a new electrochemical mass spectrometry (EC-MS) configuration. The new set-up has the same working principle as the on-line electrochemical mass spectrometry developed by Y. Gao et al. in the 1994 [34]. However, there are two main differences between both set-ups: the new EC-MS is handier and easier to build up than the described in Ref. [34]. Briefly, the analysis system is a commercial one (Omnistar™, Pfeiffer) that contains a capillary made of stainless steel as gas inlet, which was replaced by a commercial PTFE capillary (Supelco, length: 80 cm, OD: 1.56 mm and ID: 0.30 mm). The small inlet tip

consists of a porous PTFE membrane (Gore-Tex) positioned onto the PTFE capillary and fixed by a PTFE holder (Scheme 1). Thus, the PTFE membrane works as interface between the vacuum of the mass spectrometer and the electrolyte.

The set-up allows the use of massive electrodes such as single crystals and mesoporous materials as well as well-dispersed materials such as fuel catalysts (i.e. carbon supported materials, [35]). It is versatile since the high flexibility of the PTFE capillary allows different arrangements. For example, the inlet tip can be positioned close to the surface of an electrode in hanging meniscus configuration or just in the opposite way (see Scheme 1) that allows higher sensitivity and lower response time [35]. In this context, the new EC-MS system opens new avenues of research that are not only limited to electrochemical experiments. Further information on this set-up is given in [35].

With this EC-MS set-up, mass spectrometry cyclic voltammograms (MSCVs) and mass transients (MST) can be recorded simultaneously with the CVs and CTs, respectively.

2.4. EC-MS calibration

CO_2 and CH_3CHO are produced during the ethanol electrooxidation and both compounds contribute to the signal m/z = 44 ($CO_2^{\cdot+}$ and $CH_3CHO^{\cdot+}$ fragments, respectively). For this reason, the m/z = 22 signal (CO_2^{++}) was used instead of m/z = 44 to follow, distinguish and quantify the amount of CO_2 produced. The current efficiency for ethanol electrooxidation to CO_2 is determined from the subsequent equation (12 electrons per molecule of ethanol):

$$E^{CO_2} = \frac{6Q_i}{K_{22}^{*}Q_f} \quad (1)$$

where Q_f and Q_i are the faradaic charge and the ionic charge calculated from the integration of the CVs and mass spectrometric cyclic voltammograms (MSCVs) for m/z = 22, respectively, simultaneously recorded during the ethanol oxidation reaction. The factor 6 is related to the number of electrons required to produce a molecule of CO_2 during the alcohol oxidation. K_{22}^{*} is the calibration constant for the m/z = 22 signal, which is calculated from a CO stripping experiment through the following expression:

$$K_{22}^{*} = \frac{2Q_i}{Q_f} \quad (2)$$

where Q_f and Q_i are the faradaic charge and the ionic charge for m/z = 22, respectively, simultaneously recorded during the oxidation of a monolayer of adsorbed CO (CO_{ad}) to CO_2. The factor 2 is associated to the number of electrons required to produce a molecule of CO_2 during the CO_{ad} oxidation reaction.

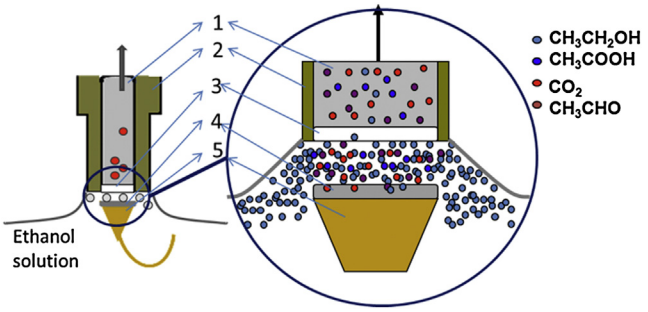

Scheme 1. The image shows the principal characteristics of the new EC-MS configuration. 1. PTFE capillary, 2. PTFE Cone-shape Tip, 3. Hydrophobic porous PTFE membrane, 4. MPPt electrode, 5. Au wire (electrical contact).

3. Results and discussion

3.1. CO stripping

Since adsorbed CO is a strong catalyst poison and it is also a reaction intermediate during the ethanol electrooxidation reaction, its removal from the catalyst surface (denoted as CO stripping) is a key factor to be investigated [8,10,14,21,25–27]. Furthermore, the CO stripping is a powerful technique for the surface morphology and structure study. In addition, CO stripping is a convenient technique to obtain an accurate estimation of the ESA [8,9].

Fig. 1 shows the CO stripping voltammogram and the subsequent CVs recorded for the MPPt catalyst in acidic medium at a scan rate of 5 mV s^{-1} (black lines). Additionally, the MSCVs achieved with ionic currents that are associated to carbon dioxide formation (m/z = 22 and 44) are also depicted in Fig. 1. The second CV resembles that previously reported for MPPt surfaces in acidic medium [10]. Thus, the voltammogram shows the presence of reversible current peaks at 0.12 and 0.27 V, which are related to H adsorption/desorption on sites with (110) and (100) orientation, respectively [21]. Additionally, it is clearly observed the onset for the Pt surface oxidation at higher potentials than 0.6 V, which is reduced during the backward scan from 1.0 to 0.6 V.

On the other hand, it is established that the onset potential for the CO oxidation reaction on MPPt catalyst occurs at ca. 0.4 V and that the well-known "pre-peak" appears in this case as an anodic constant current that extends until ca. 0.6 V. The cause of the "pre-peak" has been largely discussed using Pt single crystals in acidic and alkaline media [9,13,21,36–43], and the enhanced catalytic activity toward the CO tolerance was tentatively related to an easily water dissociation on "special sites" such as low-coordinated atoms (atoms situated at border, step, edge, or kink sites), in which the local electronic density is highly altered. Therefore, the charge density under the "pre-peak" region observed at the MPPt catalyst has to be associated to the CO oxidation at very active sites presumably situated onto the concave structure of the electrode. At more positive potentials the complete CO removal occurs developing an anodic peak centered at ca. 0.68 V [10,37]. Then, it is normally accepted that the electrooxidation of adsorbed CO follows a Langmuir–Hinshelwood mechanism, in which the first

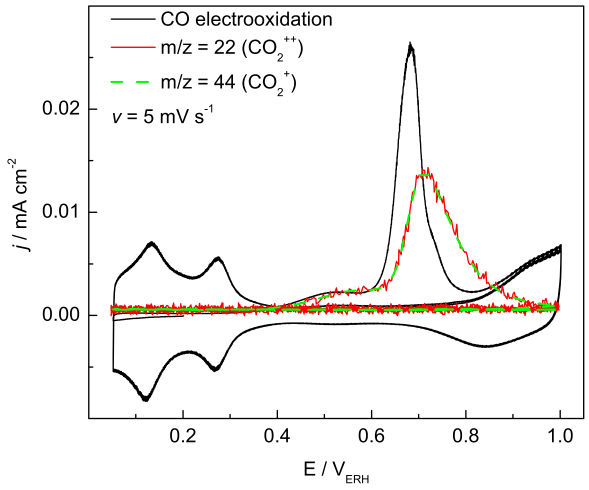

Fig. 1. CO stripping CV and MSCV. Faradaic current density (black) and ionic current density of m/z = 22 and 44 (red and green) registered during the electrooxidation of a CO_{ad} monolayer on MPPt electrode in 0.5 M H_2SO_4. v = 5 mV s^{-1}; T = 25 °C. The CO_2^{++} and CO_2^{+} current signals were adjusted by the K_{22}^{*} and K_{44}^{*}, respectively.

reaction should be the formation of oxygenated species on the surface [38,39]:

$$Pt + H_2O \rightarrow Pt\text{-}OH + H^+ + e^- \quad (1)$$

$$Pt\text{-}CO + Pt\text{-}OH \rightarrow Pt\text{-}COOH + Pt \quad (2)$$

$$Pt\text{-}COOH \rightarrow CO_2 + H^+ + e^- + Pt \quad (3)$$

The signals for m/z = 22 (CO_2^{++}) and m/z = 44 (CO_2^{+}), which are detected at the mass spectrometer, are both associated to the formation of carbon dioxide during the CO_{ad} electrooxidation reaction. Faradaic current can be calculated from the calibration constant for the m/z = 22 (K_{22}^{*}) as was described above (section 2.4). The shift for the main CO_{ad} oxidation peak to higher potentials in the MSCVs can be explained in terms of the impeded diffusion of relatively high amount of CO_2 from the mesoporous structure of the catalyst, which partially delays the detection at the mass spectrometer. However, it is observed that the m/z = 22 and 44 signals decay to zero indicating that all CO_2 produced is detected during the positive-going scan.

In this context, the high precision of the new EC-MS set-up allows the detection of the onset potential for the CO oxidation reaction with great exactitude (no shift is expected in the signals at the onset potential as only small amounts of CO_2 are formed and diffusion is not constrained). Thus, from these results it can be concluded that after the correct calibration of the EC-MS system, becomes feasible to study the reaction mechanism and to achieve the ethanol conversion efficiency to CO_2. It is remarkable that a complete on-line detection of the CO stripping (with no shift in the peak potential) is recorded when this configuration is used for the study of carbon supported materials with the same EC-MS (see [35] for more details), so the shift in Fig. 1 has to be related to the electrode morphology.

3.2. Ethanol electroreactivity

3.2.1. CVs and MSCVs for MPPt in 0.01 CH_3CH_2OH + 0.5 M H_2SO_4 solution

Fig. 2 shows the first two CVs and the corresponding MSCVs for the m/z = 22 (CO_2^{++}), m/z = 29 (CHO^+) and m/z = 15 (CH_3^+) signals during the electrooxidation of 0.01 M ethanol at the MPPt electrode in acidic media recorded at 2 mV s^{-1}. The signals for m/z = 22 and 29 are related to carbon dioxide and acetaldehyde formation, respectively, while the m/z signal 15 is associated to methane and acetaldehyde production (CH_3^+ fragment from both compounds) at low (E < 0.5 V in the forward scan and E < 0.3 V in the negative sweep) and high (E > 0.5 V in the forward scan and E > 0.3 V in the negative sweep) potentials, respectively. The signal for m/z = 15 could be associated to the production of acetaldehyde in the whole potential range, but a close comparison of the MSCVs for m/z = 15 and 29 (the latter only related to acetaldehyde), shows that both MSCVs are similar for E > 0.5 V but at E < 0.5 V the features in the MSCV for m/z = 15 are not present for m/z = 29. Therefore, in this potential range the signal for m/z = 15 has to be related to the formation of a different compound, in this case methane (this difference is even more apparent for 0.1 M ethanol concentration, see Fig. 4 middle panels). It is remarkable that methane formation on carbon supported Pt during the forward scan of ethanol electrooxidation in the 0.2-0.5 V potential range has been reported for the first time by our group [35]. As in that case, methane is also produced in the same potential region at MPPt.

It is important to take into account that the ethanol solution was introduced into the cell at a controlled working electrode

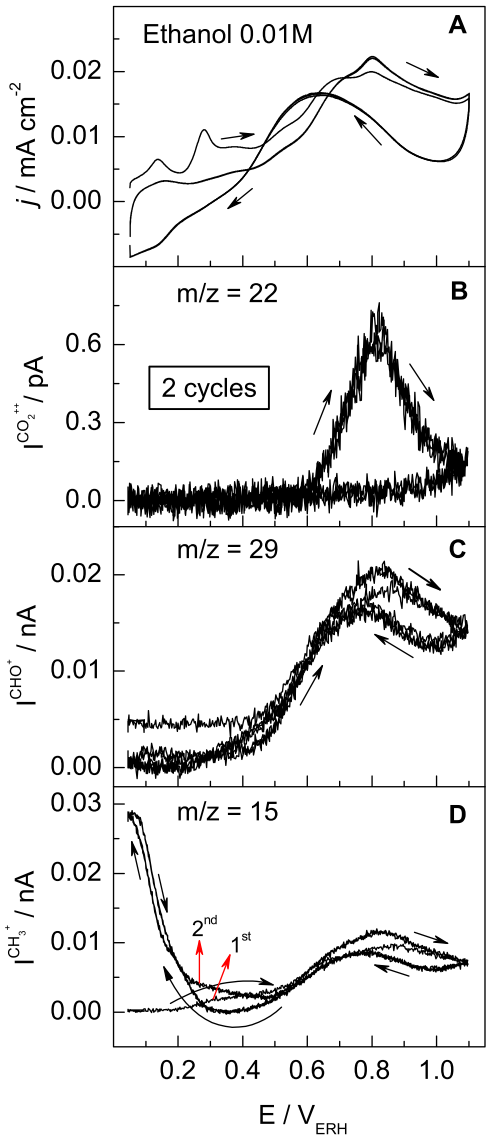

Fig. 2. Ethanol electrooxidation on MPPt catalyst in 0.01 M ethanol + 0.5 M H_2SO_4. CVs (A) and MSCVs for m/z = 22 (B), m/z = 29 (C) and m/z = 15 (D). ν = 2 mV s^{-1}; T = 25 °C.

potential of 0.05 V. Therefore, a competitive adsorption between hydrogen and ethanol is expected during the first potential-going scan from 0.05 V upwards [15,26,29]. A detailed view of the first positive-going scan (Fig. 2A) suggests two potential regions, which account for the two main steps of the ethanol oxidation reaction. First, ethanol electrosorption and dehydrogenation steps occur at E < 0.38 V, and the delivered faradaic current in this potential region is related to the hydrogen desorption, ethanol adsorption/dehydrogenation reactions and methane formation. At higher potentials, electrooxidation takes place. A close view of the m/z = 29 and m/z = 15 signals indicate that the onset potentials for acetaldehyde and methane formation are located at 0.38 and 0.2 V, respectively. Moreover, the onset potentials for methane and acetaldehyde coincide with the completion of hydrogen desorption on Pt sites with (110) and (100) orientation, respectively.

In this context, it can be concluded that the dissociative adsorption of ethanol on MPPt at low potentials is not obstructed by the high degree of adsorbed hydrogen, in contrast to what is

reported for alcohols on other type of Pt structures [26,27,40–43]. On the other hand, in agreement with previous studies, the results depicted in Fig. 2 indicate that breaking of the C-C bond of ethanol molecule can occur at E < 0.5 V and partial oxidation at E > 0.38 V [35]. Other details of the ethanol oxidation reaction mechanism will be described below.

The electrooxidation of ethanol to acetaldehyde is visible at E > 0.38 V (signal for m/z = 29), while the electrooxidation of ethanol fragments (e.g. CO_{ad}) to produce CO_2 (signal for m/z = 22) is apparent at E > 0.5 V. Interestingly all signals (ionic and faradaic currents) develop a peak at ca. 0.8 V, which is close to the onset potential for water dissociation on platinum surface, i.e. OH_{ad} formation (Reaction (1)). At potentials higher than 0.8 V, the signal associated to carbon dioxide formation falls to zero, meanwhile the signal related to acetaldehyde decreases. It is well known that alcohol adsorption is inhibited at platinum oxides surface, and consequently, the lower activity toward the ethanol oxidation at these positive potentials is attributed to this fact.

Acetic acid cannot be easily detected by DEMS. However, it can be indirectly followed by the signals m/z = 43, 61 and 73 due to a chemical reaction of the generated acid with ethanol forming the corresponding ester at high ethanol concentrations, as will be discussed in the subsequent Section (3.2.3).

During the backward scan, an increment of the faradaic current and acetaldehyde signals (m/z = 15 and 29) is observed between 1.0 and 0.75 V. This behavior is related to surface Pt oxides reduction accompanied with ethanol re-adsorption, which finally reacts again. Then, the rate of acetaldehyde formation decreases at E < 0.75 V. In addition, the profile of the m/z = 22 signal during the backward scan indicates that almost no carbon dioxide is produced. The last must be associated to negligible C-C bond breaking of the alcohol during the negative-going potential sweep in this potential region. Furthermore, subsequent potentiodynamic cycles for m/z = 22 display the same mass spectrometric profiles, which indicates that equal amount of adsorbed ethanol residues are formed in each cycle. As will be described below, the yield of carbon dioxide is almost independent of ethanol concentration, a fact that can be taken as an indication that CO_2 is mainly produced from the adsorbed species formed on the Pt surface at low potentials.

On the other hand, the MSCV for m/z = 15 (CH_3^+) shows a similar profile to the mass m/z = 29 at E > 0.5 V, and therefore, can be ascribed to acetaldehyde production. However, the profile is completely different during the backward scan and subsequent scans at E < 0.38 V, in which a strong increment of the m/z = 15 signal is discerned. In this context, the rise of this signal at E < 0.38 V is associated to the formation of methane, and consequently, CO_{ad} is expected as adsorbed intermediate from the C-C scission of the ethanol molecule. However, the production of ethane was also observed in this potential region through the signal for m/z = 30 ($C_2H_6^+$) (see later, Fig. 6) indicating that C_2-adsorbed species are also formed.

Then, a variety of adsorbed species different and less oxidized than CO_{ad} are present on the catalysts surface, being probably responsible for the low oxidation efficiencies obtained for ethanol electrooxidation to CO_2. According to these results, it is concluded that the m/z = 15 signal follows both acetaldehyde and methane formation on MPPt electrode at higher and lower potentials than 0.3 V, respectively.

3.2.2. CVs and MSCVs for MPPt in 0.01-1.0 CH_3CH_2OH + 0.5 M H_2SO_4 solutions

In order to study the effect of ethanol concentration during the alcohol oxidation reaction at MPPt electrode, several ethanol solutions were employed. Fig. 3 depicts the CVs and MSCVs (m/z = 22 and 44) for the electrooxidation of ethanol (0.01–1.0 M) on

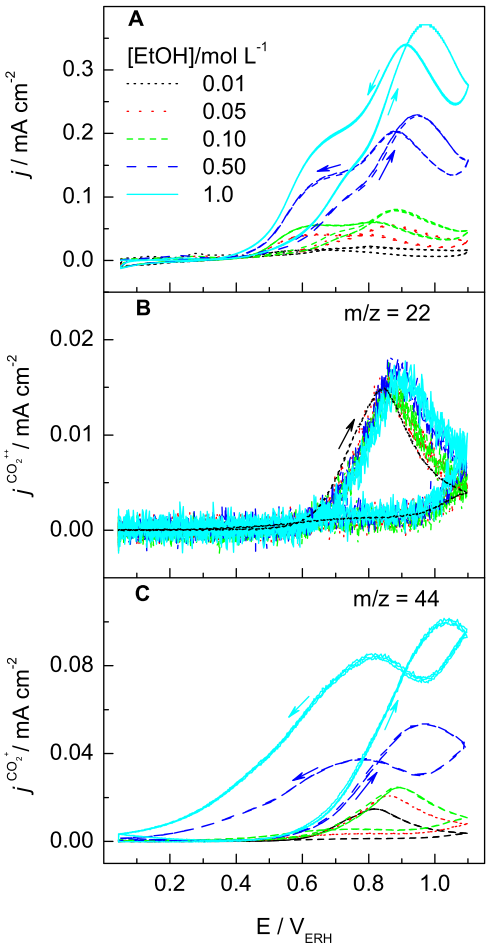

Fig. 3. Ethanol electrooxidation on MPPt in different ethanol concentrations as indicated. CVs (A) and MSCVs for m/z = 22 (B) and m/z = 44 (C) $v = 2$ mV s^{-1}; T = 25 °C. The CO_2^{++} and CO_2^{+} current signals were adjusted by the K_{22}^{*} and K_{44}^{*}, respectively.

MPPt in acidic medium. It can be observed a strong increment of the faradaic current and the m/z = 44 signal with the rise of the alcohol concentration. It is noticeable that the m/z = 44 signal can be related to acetaldehyde (CH_3CHO^+) and/or carbon dioxide formation (CO_2^+). However, the m/z = 22 signal, associated only to carbon dioxide production, remains almost constant with the increment of the alcohol concentration. Therefore, the rise of the faradaic current with the ethanol concentration must be related to an increment of by-side reactions, such as acetaldehyde (and acetic acid) production.

In order to confirm the stated above, the ethanol oxidation reaction on MPPt in acidic media was monitored with the mass signals for m/z = 15 and 29 and the alcohol concentration was varied. Fig. 4 shows the first two CVs and the corresponding MSCVs for the m/z = 22 (CO_2^{++}), m/z = 15 (CH_3^+) and m/z = 29 (CHO^+) signals during the electrooxidation of three different concentration of ethanol (0.01, 0.1 and 1.0 M) at the MPPt electrode in acidic media recorded at 2 mV s^{-1}. It can be discerned in the CVs that the current density increases and the main anodic peak shifts toward more positive potentials with the rise of alcohol concentration. In this context, the acetaldehyde production (m/z = 29) and the faradaic current follow similar profiles (as well as the signal for m/z = 44 in Fig. 3), and it is observed that 10-fold increase in ethanol concentration produces a 10-fold increase of the m/z = 29 signal. The ion current associated to the m/z = 15 signal increases as the m/

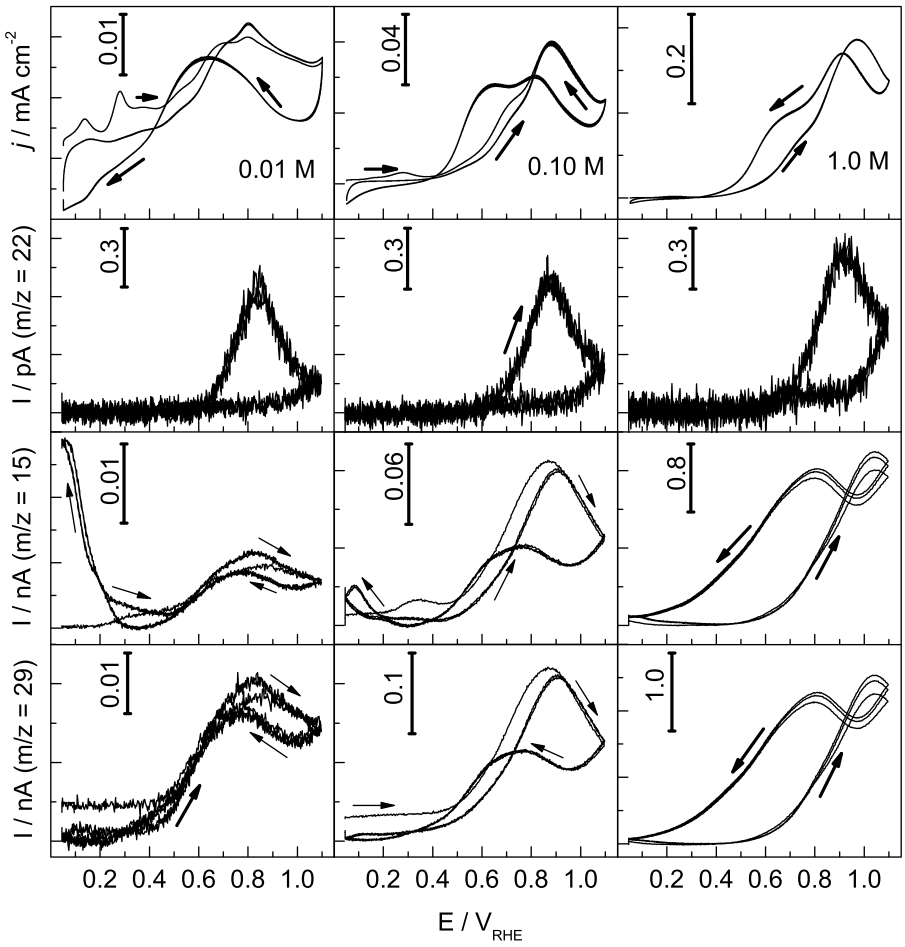

Fig. 4. CVs (top panel) and MSCVs (bottom panel: m/z = 15) of ethanol electrooxidation on MPPt in 0.01, 0.1 and 0.5 M ethanol electrooxidation on MPPt in 0.5 M sulphuric acid solution. $v = 2\ mV\ s^{-1}$; T = 25 °C.

z = 29 signal at higher potentials than 0.5 V with the rise of the alcohol concentration.

Interestingly, the amount of methane formation (m/z = 15) between 0.2 and 0.45 V during the first forward scan also increases 10-fold with the rise of ethanol concentration from 0.01 to 0.1 M (see Fig. 5 for a magnification of the signal in this potential region). However, the intensities of the m/z = 15 signal at E < 0.3 V during the negative sweep and subsequent scans are not (or slightly) affected by the ethanol concentration. The same occurs with the MSCV for m/z = 22. The last behavior indicates that the CH_4 and CO_2 formation, and consequently the C-C bond breaking, is nearly independent of the ethanol concentration after the first positive scan, in agreement with previous results achieved at carbon supported Pt catalysts [27].

The formation of acetic acid from the ethanol oxidation reaction in acidic medium can be followed indirectly, for example by the signal for m/z = 61 ($C_2H_5O_2^+$) (middle panel of Fig. 6). As was described above, the dissociation and lower volatility of acetic acid makes impossible its detection by EC-MS and therefore another strategy must be adopted. In this context, it is well known that ethyl acetate ester can be produced from the chemical reaction occurring between ethanol and acetic acid in low pH solutions:

$$CH_3COOH + CH_3CH_2OH \rightleftharpoons CH_3COOCH_2CH_3 + H_2O \quad (4)$$

Thus, ethyl acetate ester is a volatile molecule that can be identified by EC-MS and the m/z = 43, 61 and 73 signals (the last two in Fig. 6) are usual ionic fragments of ethyl acetate to follow during the ethanol oxidation reaction [25,44]. However, the detection time at the mass spectrometer is quite high and an accurate measurement is not possible (see the delay time between the CV and the MSCV). The last is associated to several effects such as the diffusion time from the bulk solution (Reaction (4) is not a surface but a bulk solution reaction) to the PTFE membrane, the low permeability of the ethyl acetate ester through the PTFE membrane, as well as, the reaction rate of the Eq. (4) [20]. As an equilibrium reaction, it is shifted to the right at high ethanol concentrations. Thus, acetic acid formation can only be indirectly followed by EC-MS at 1.0 M ethanol concentration.

3.2.3. Chronoamperometric studies for MPPt electrode in 0.01-1.0 CH_3CH_2OH + 0.5 M H_2SO_4 solution. Efficiencies for ethanol conversion to CO_2

Potentiostatic measurements allow a more precise determination of the conversion efficiency for the ethanol oxidation reaction at relevant voltage values for DAFCs, as the problems associated with the slow diffusion of CO_2 from the MP structure to be detected are avoided if enough recording time is considered. Fig. 7 depicts the current transients (CTs) and mass spectrometric current transients (MSCTs) recorded at different applied potentials and several ethanol concentrations in sulphuric acid medium. In agreement with the MSCVs for the m/z = 22 signal (Figs. 3 and 4), carbon dioxide formation is not observed in Fig. 7 at lower

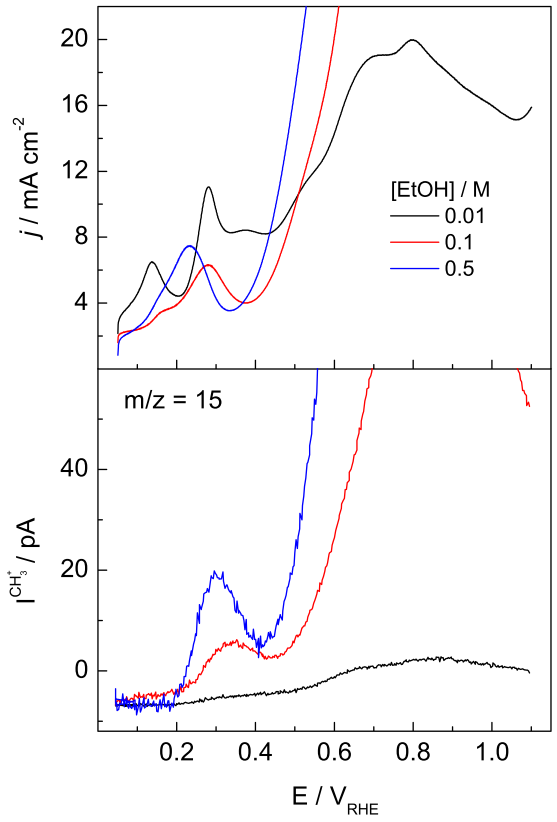

Fig. 5. CVs (top panels) and MSCVs (middle panels: m/z = 22 and 15; bottom panels: m/z = 29) of ethanol electrooxidation on MPPt in 0.01, 0.1 and 1 M ethanol electrooxidation on MPPt in 0.5 M sulphuric acid solution. v = 2 mV s^{-1}; T = 25 °C.

potentials than 0.6 V and its production is almost constant with all ethanol concentrations analyzed. On the other hand, the m/z = 29 signal related to acetaldehyde production increases with the rise of the applied potential and the ethanol concentration, also in good agreement with the voltammetric study described above (Figs. 3 and 4). These results confirm that the partial oxidation of ethanol to acetaldehyde (and presumably acetic acid) is the main contribution to the overall faradaic current. On the other hand, it is noticeable the close correlation between faradaic and ionic currents, which indicates the great performance of the novel EC-MS configuration.

Table 1 shows the efficiencies for ethanol conversion to CO_2 (E^{CO2}) calculated for different alcohol concentrations at 0.6 and 0.7 V. In agreement with the potentiostatic and potentiodynamic studies, the highest E^{CO2} (11.1%) is achieved at 0.6 V with the lowest ethanol concentration utilized (0.01 M), and it decreases with increasing the potential and the rise of alcohol concentration. In this context, alcohol concentration above 0.1 M may decrease the CO_2 mass signal detection in the mass chamber and therefore small deviations of the E^{CO2} may be obtained at elevated ethanol concentrations [45]. However, in the configuration used in this paper the pressure of the mass chamber can be monitored and recorded on real time and therefore the mass current signals can be normalized with the real mass chamber pressure and a high accuracy is attained.

3.2.4. Kinetics and reaction mechanism of ethanol electrooxidation at MPPt

In agreement with the results showed above and those in the literature [35,44,46–52], we are in conditions to give a global description of the ethanol adsorption, oxidation and reduction processes at MPPt electrode. It is well known that saturated alcohol molecules have two reactive sites, the OH group and the α-carbon atom, that can interact with the Pt surface during the adsorption process:

$$Pt + CH_3CH_2OH \rightleftharpoons Pt(CH_3CH_2OH) \quad (5)$$

$$Pt(CH_3CH_2OH) \rightarrow Pt\text{-}OCH_2CH_3 + H^+ + e^- \quad (6)$$

$$Pt(CH_3CH_2OH) \rightarrow Pt\text{-}CHOHCH_3 + H^+ + e^- \quad (7)$$

These reactions can be considered the starting steps for the ethanol electrooxidation reaction. These processes occur during the positive scan as soon as free Pt sites are available once hydrogen starts to be desorbed. The ethoxi species $Pt\text{-}OCH_2CH_3$ is relatively stable, whereas the alcohol derivative $Pt\text{-}CHOHCH_3$ easily dehydrogenates [17] finally producing acetaldehyde:

$$Pt\text{-}CHOHCH_3 \rightarrow Pt(HCOCH_3) + H^+ + e^- \quad (8)$$

$$Pt(HCOCH_3) \rightleftharpoons Pt + HCOCH_3 \quad (9)$$

Both adsorbed ethoxi and alcoholic C_2-intermediates were previously detected at polycrystalline Pt by FTIRS [17,50]. Reactions (7)–(9) are the main responsible for the delivered current and **acetaldehyde production** at potentials higher than 0.38 V (in the absence of adsorbed hydrogen) and are strongly dependent on the ethanol concentration.

However, during the first positive potential going scan between 0.05 and 0.38 V, it can be assumed that ethanol initially adsorbs at Pt(110) sites as soon as this sites become free of H_{ad} and the alcohol intermediate formed in Reaction (7) reacts with H_{ad} still present at (100) sites producing methane:

$$Pt_{100}(H) + Pt\text{-}CHOHCH_3 \rightarrow Pt\text{-}CO + CH_4 + 2H^+ + 2e^- \quad (10)$$

This reaction accounts for **methane production** observed **in the first anodic scan in the 0.2-0.4 V potential range** (Fig. 5), and as in the case of Reactions (7)–(9), is strongly dependent on ethanol concentration. It is noteworthy that Reaction (10) is in agreement with FTIRS experiments in which **adsorbed carbon monoxide** on Pt single crystals was detected at similar potentials [22]. However, FTIRS is not able to detect methane since a change in the dipole moment should occur for a vibration to be infrared active.

On the other hand, if free Pt sites are available, further deprotonation of alcohol species is possible according to:

$$Pt\text{-}CHOHCH_3 + Pt \rightarrow Pt_2\text{-}COHCH_3 + H^+ + e^- \quad (11)$$

This new adsorbate cannot be desorbed as acetaldehyde and will be finally oxidized to CO_2 (see Scheme 2) in the positive run. Moreover, further scission of the C-C bond can occur through the reaction:

$$Pt_2\text{-}COHCH_3 \rightarrow Pt\text{-}CH_3 + Pt\text{-}CO + H^+ + e^- \quad (12)$$

During the reverse scan, adsorption and deprotonation of ethanol with the formation of species in Reactions (11) or (12) can occur as soon as the reduction of Pt oxides takes place, although in this case ethanol adsorption is not limited to Pt(110) sites.

The **production of methane in the hydrogen potential region during the backward scan** (see Fig. 4) can be formed with the interaction of the methyl residue formed in Reaction (12) with H_{ad}, independently of the Pt surface site structure.

$$Pt\text{-}CH_3 + Pt\text{-}H \rightarrow CH_4 \quad (13)$$

It is remarkable that the yield to methane during the negative-going potential scan is practically independent of the ethanol

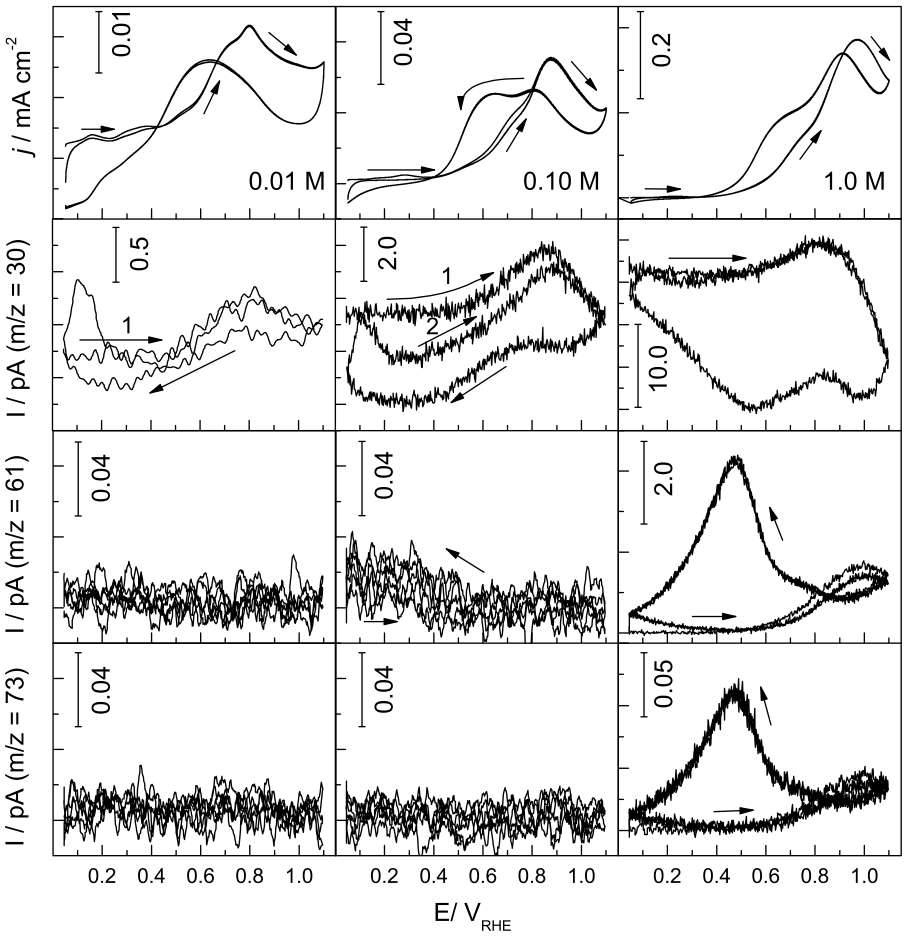

Fig. 6. CVs (top panels) and MSCVs (middle panels: m/z = 30 and 61; bottom panels: m/z = 73) of ethanol electrooxidation on MPPt in 0.01, 0.1 and 1 M ethanol electrooxidation on MPPt in 0.5 M sulphuric acid solution. v = 2 mV s^{-1}; T = 25 °C.

concentration. The last indicates that methane is mostly produced from the adsorbed species formed on the MPPt electrode in Reaction (12).

In addition, it was observed that **carbon dioxide** is mainly **produced during the forward scan**, is practically independent of ethanol concentration and its amount is equal in every potentiodynamic cycle. These facts can be taken as an indication that CO_2 is mainly produced from the adsorbed species (Pt-CH_3 and Pt-CO formed from Pt_2-$COHCH_3$) formed on the MPPt surface. CO_{ad} removal occurs through the Reactions (1)–(3), while the complete oxidation reaction of adsorbed CH_3 species may occur in the following way:

$$Pt\text{-}CH_3 + 2Pt\text{-}OH \rightarrow CO_2 + 5H^+ + 5e^- + 3Pt \quad (14)$$

It is necessary to mention that Reaction (14) does not represent the elementary steps of the oxidation of adsorbed CH_3 species, which probably involves a CO-like intermediate [51].

On the other hand, it was proposed in [48] that adsorbed acetaldehyde is responsible for **ethane formation** during the excursion to negative potentials when acetaldehyde was adsorbed on Pt at E > 0.3 V. But in that study, ethane was detected only when the applied potential was in the region of hydrogen evolution, other way only methane was detected. Nevertheless, in the current work the onset for ethane production on MPPt is observed at 0.2 V during the negative-going potential scan attaining a maximum at 0.1 V during the forward run. Accordingly, the following reaction appears to be the more suitable for ethane formation in this potential region, in agreement with a previous work on ethanol adsorption [17]:

$$Pt_2\text{-}COHCH_3 + 4Pt\text{-}H \rightarrow CH_3CH_3 + H_2O + 6Pt \quad (15)$$

$$Pt\text{-}COHCH_3 + 4Pt\text{-}H \rightarrow CH_3CH_3 + H_2O + 5Pt \quad (16)$$

Finally, **acetic acid formation** is detected by EC-MS at E > 0.6 V during the forward sweep and also during the reverse scan. Thus, this reaction can be written as a direct reaction of adsorbed acetaldehyde with adsorbed oxygenated species (OH_{ad}) on the metallic substrate:

$$Pt(HCOCH_3) + Pt\text{-}OH \rightarrow CH_3COOH + H^+ + e^- + 2Pt \quad (17)$$

The Scheme 2 will assist in summarizing the principal reaction pathways of the ethanol reactivity on MPPt in acidic media.

Finally, some kinetic information can be obtained from chronoamperometric measurements. Tafel plots (Fig. 8) were calculated from stationary faradaic (top panel) and ionic currents (bottom panel) achieved at 300 s during the current-time experiments. The m/z = 15, 29 and 44 signals were acquired in 0.05 M ethanol solution. In order to attain detectable ionic currents, the signal associated to acetic acid (m/z = 61) was obtained in 1 M ethanol solution. Tafel slopes of 120 mV dec^{-1} were achieved for the faradaic currents independently of the ethanol concentration at E ≤ 0.6 V. Likewise, the m/z = 29 signal related to acetaldehyde formation perfectly match with a Tafel slope of 120 mV dec^{-1} in the

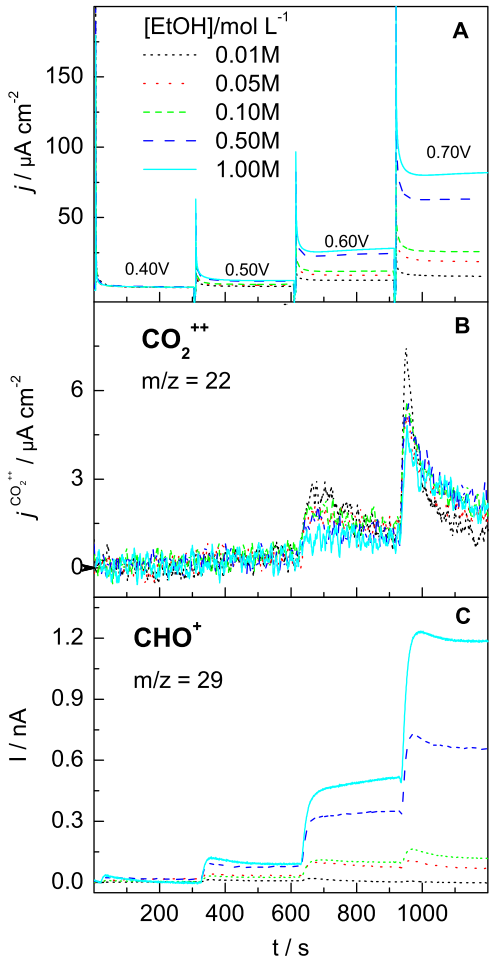

Fig. 7. CTs (A) and MSCTs for m/z = 22 (middle panel) and m/z = 29 (bottom panel) of 0.01, 0.05, 0.1, 0.5, and 1 M ethanol electrooxidation on MPPt in 0.5 M sulphuric acid solution. Potentials steps from 0.05 V to 0.4, 0.5, 0.6 and 0.7 V. T = 25 °C. The CO_2^{++} current signal was adjusted by the K_{22}^{*}.

same potential range. The signals for m/z = 15 and 44 show slightly higher Tafel slopes (~130 mV dec^{-1}) at E ≤ 0.6 V and that related to acetic acid production (m/z = 61) develops the highest Tafel slope (140 mV dec^{-1}). The small deviation for the former mass to charge ratios can be associated to the fact that these signals are not only associated to acetaldehyde but also to methane (m/z = 15) and carbon dioxide (m/z = 44), whereas the low accuracy for m/z = 61 (see explanation of Reaction (4) appears as the main responsible for this signal.

Therefore, assuming that all faradaic and ionic currents develop similar Tafel slope (~120 mV dec^{-1}) at E ≤ 0.6 V, the reaction mechanism as well as rate-determining step (*rds*) involved in the ethanol oxidation can be proposed. Indeed, it is noticeable that all signals deviate from the linearity at E = 0.7 V, potential in which the strongly adsorbed ethanol residues (CO and CH_3) can be removed from the Pt surface. Thus, it is expected that ethanol adsorbs

Table 1
Efficiency of ethanol conversion to CO_2 (E^{CO2}) at MPPt catalyst recorded at 0.60 and 0.70 V in 0.5 M sulphuric acid solution.

[EtOH]/mol L^{-1}	E^{CO2} (0.60 V)	E^{CO2} (0.70 V)
0.01	11.1	9.4
0.05	5.5	4.6
0.10	4.6	3.8
0.50	1.8	1.6
1.00	1.2	1.1

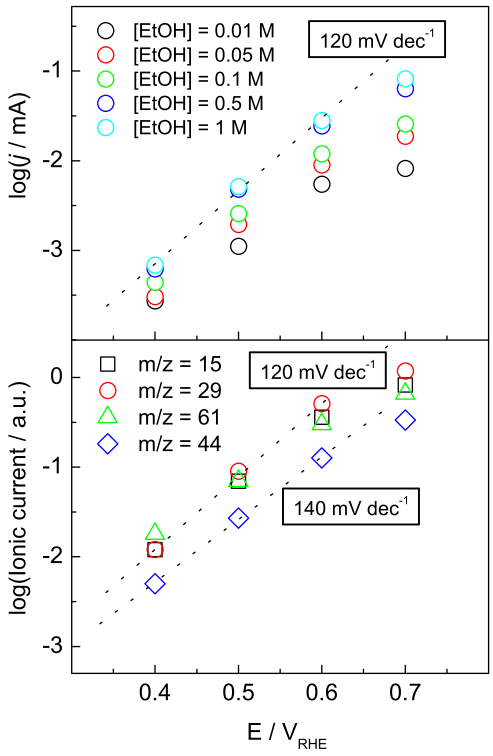

Fig. 8. Tafel plots of the CTs (upper panel) and MCTs (bottom panel) on the MPPt electrode.

dissociatively on the MPPt electrode at low overpotentials leading adsorbed CO and CH_3 fragments on the catalyst surface. These residues are slowly oxidized at lower potentials than 0.6 V, and hence the water dissociation (Reaction (1)) appears as the *rds* to fulfill the mechanism reaction for the whole ethanol oxidation reaction [53].

A deeply analysis can be carry out using the ionic currents recorded for m/z = 29 signal which is only related to acetaldehyde. It is important to recall that ethanol dehydrogenation leads acetaldehyde (Reactions (7) and (8)) without the need of adsorbed oxygenated species (OH_{ad}). This signal also develops a Tafel slope value of 120 mV dec^{-1}, which must be associated to the first electrochemical step as the *rds*. Thus, Eq. (7) (the first dehydrogenation step) emerges as the *rds* for the electrochemical production of acetaldehyde species.

4. Conclusions

A new electrochemical mass spectrometry (EC-MS) configuration was developed and applied to different catalysts. It was proved that the novel EC-MS is a valuable and versatile technique with high accuracy and facile to build-up.

A deep fundamental study devoted to establish the reaction mechanism and the kinetics for the ethanol oxidation on MPPt catalyst was successfully investigated by combining electrochemical techniques with the new EC-MS set-up. In this context, methane formation during the positive scan between 0.2 and 0.4 V on MPPt is for the first time reported. This result is of paramount importance since new insights of the ethanol oxidation reaction are revealed.

Finally, a profound applied work related to energy generation throughout the fuel cell technology was carried out and the energy conversion efficiency from ethanol to CO_2 was calculated. Main results indicate an increment of by-side products (acetaldehyde and acetic acid) with the rise of the alcohol concentration.

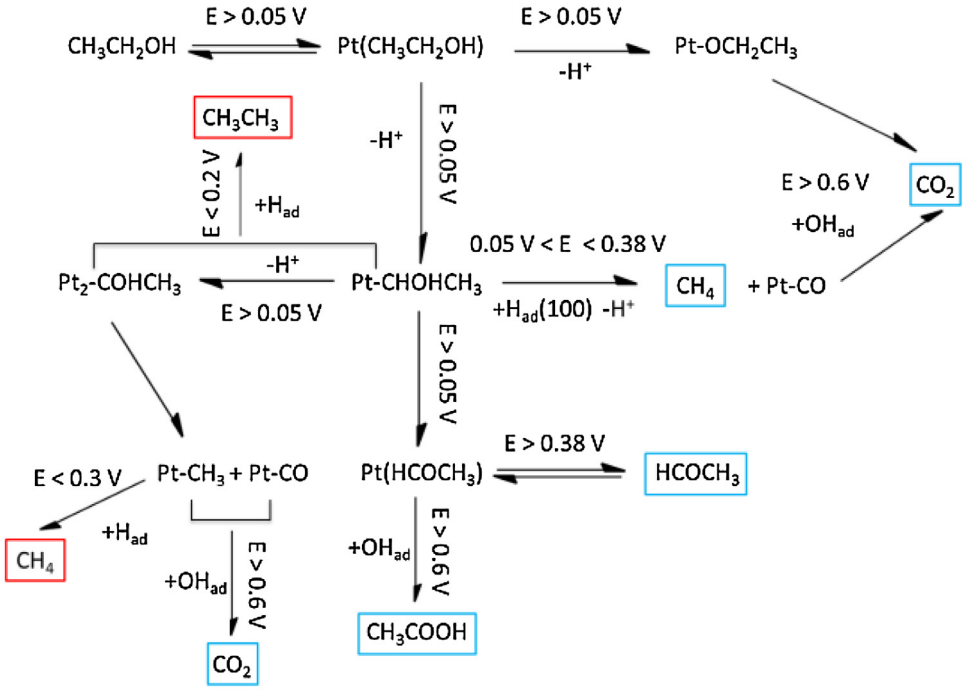

Scheme 2. Reaction mechanism of the ethanol oxidation on MPPt electrode in acidic medium. Species inside the red and light blue boxes are produced during the backward and forward scans, respectively. Although no indicated for the sake of simplicity, $HCOCH_3$ and CH_3COOH are also formed during the negative-going scan.

Consequently, the highest energy conversion efficiency to CO_2 (~11%) was achieved at 0.6 V with the lowest alcohol concentration employed (0.01 M).

Acknowledgements

This work has been supported by Fundación Cajacanarias (project BIOGRAF). J. Flórez-Montaño thanks ACIISI (Gobierno de Canarias) for the pre-doctoral fellowship and BIOGRAF for the research contract.

References

[1] E. Antolini, Catalyst for direct ethanol fuel cells, J. Power Sources 170 (2007) 1–12.
[2] C. Lamy, E.M. Belgsir, J.M. Leger, Electrocatalytic oxidation of aliphatic alcohols: Application to the direct alcohol fuel cell (DAFC), J. Appl. Electrochem. 31 (2001) 799–809.
[3] B. Braunchweig, D. Hibbitts, M. Neurock, A. Wieckowski, Electrocatalysis: A direct alcohol fuel cell and surface science perspective, Catal. Today 202 (2013) 197–209.
[4] L. Zhang, W.X. Niu, G.B. Xu, Seed-mediated growth of palladium nanocrystals: The effect of pseudo-halidethiocyanate ions, Nanoscale 3 (2011) 678–682.
[5] Y.W. Lee, S.B. Han, D.Y. Kim, K.W. Park, Monodispersed platinum nanocubes for enhanced electrocatalytic properties in alcohol electrooxidation, Chem. Commun. 47 (2011) 6296–6298.
[6] J.M. Elliott, G.S. Attard, P.N. Bartlett, N.R.B. Coleman, D.A.S. Merckel, J.R. Owen, Nanostructured platinum (HI-ePt) films: Effects of electrodeposition conditions on film properties, Chem. Mater. 11 (1999) 3602–3609.
[7] N. Menzel, E. Ortel, R. Kraehnert, P. Strasser, Electrocatalysis using porous nanostructured materials, ChemPhysChem 13 (2012) 1385–1394.
[8] M.V. Martínez-Huerta, G. García, Fabrication of electrocatalytic nanoparticles and applications to proton exchange membrane fuel cells, in: D.Y.C. Leung, J. Xuan (Eds.), Micro & Nano-Engineering of Fuel Cells (Sustainable Energy Developments), CRC Press Taylor and Francis Group, London, 2015 ISBN 0-41564-439-9.
[9] T.F. Esterle, A.E. Russell, P.N. Bartlett, Study of carbon monoxide oxidation on mesoporous platinum, ChemPhysChem 11 (2010) 2896–2905.
[10] G.A. Planes, G. García, E. Pastor, High performance mesoporous Pt electrode for methanol electrooxidation. A DEMS study, Electrochem. Commun. 9 (2007) 839–844.
[11] G. García, J. Florez-Montaño, A. Hernandez-Creus, E. Pastor, G.A. Planes, Methanol electrooxidation at mesoporous Pt and Pt–Ru electrodes: A comparative study with carbon supported materials, J. Power Sources 196 (2011) 2979–2986.
[12] J. Flórez-Montaño, G. García, E. Rodríguez, P. Pastor, G.A. Planes, On the design of Pt based catalysts. Combining porous architecture with surface modification by Sn for electrocatalytic activity enhancement, J. Power Sources 282 (2015) 34–44.
[13] H. Wang, C. Wingender, H. Baltruschat, M. Lopez, M.T. Reetz, Methanol oxidation on Pt, PtRu, and colloidal Pt electrocatalysts: A DEMS study of product formation, J. Electroanal. Chem. 509 (2001) 163–169.
[14] H. Wang, H. Abruña, in: A. Bocarsly, D.M.P. Mingos (Eds.), Electrocatalysis of direct alcohol fuel cells: Quantitative DEMS studies fuel cells and hydrogen storage, Springer, Berlin, 2011, pp. 33.
[15] M.T.M. Koper, S.C.S. Lai, E. Herrero, in: M.T.M. Koper (Ed.), Fuel Cell Catalysis—A Surface Science Approach, 192, John Wiley & Son, Inc., Hoboken, New Jersey, 2009, pp. 355.
[16] T. Iwasita, F.C. Nart, Identification of methanol adsorbates on platinum: an in situ FT-IR investigation, J. Electronal. Chem. Interf. Electrochem. 317 (1991) 291–298.
[17] T. Iwasita, E. Pastor, A dems and FTIR spectroscopy investigation of adsorbed ethanol on polycrystalline platinum, Electrochim. Acta 39 (1994) 531–537.
[18] J.M. Perez, B. Beden, F. Hahn, A. Aldaz, C. Lamy, In situ infrared reflectance spectroscopy study of the early stages of ethanol adsorption at a platinum electrode in acid medium, J. Electronal. Chem. 262 (1989) 251–261.
[19] E. Antolini, E.R. Gonzalez, A simple model to assess the contribution of alloyed and non-alloyed platinum and tin to the ethanol oxidation reaction on Pt–Sn/C catalysts: Application to direct ethanol fuel cell performance, Electrochim. Acta 55 (2010) 6485–6490.
[20] V. Bambagioni, C. Bianchini, A. Marchionni, J. Filippi, F. Vizza, J. Teddy, P. Serp, M. Zhiani, Pd and Pt–Ru anode electrocatalysts supported on multi-walled carbon nanotubes and their use in passive and active direct alcohol fuel cells with an anion-exchange membrane (alcohol = methanol ethanol, glycerol), J. Power Sources 190 (2009) 241–251.
[21] G. García, M.T.M. Koper, Carbon Monoxide Oxidation on Pt Single Crystal Electrodes: Understanding the Catalysis for Low Temperature Fuel Cells, ChemPhysChem 12 (2011) 2064–2072.
[22] S.-C. Chang, L.-W.H. Leung, M.J. Weaver, Metal crystallinity effects in electrocatalysis as probed by real-time FTIR spectroscopy: Electrooxidation of formic acid, methanol, and ethanol on ordered low-index platinum surfaces, J. Phys. Chem. 94 (1990) 6013–6021.
[23] T. Iwasita, B. Rasch, E. Cattaneo, W. Vielstich, A sniftirs study of ethanol on platinum, Electrochim. Acta 34 (1989) 1073–1079.
[24] X.H. Xia, H.-D. Leiss, T. Iwasita, Early stages in the oxidation of ethanol at low index single crystal platinum electrodes, J. Electroanal. Chem. 437 (1997) 233–240.
[25] V.M. Schmidt, R. Ianniello, E. Pastor, S. González, Electrochemical reactivity of ethanol on porous Pt and PtRu: oxidation/reduction reactions in 1 M $HClO_4$, J. Phys. Chem. 100 (1996) 17901–17908.
[26] E. Mostafa, A.A. Abd-El-Latif, R. Ilsley, G. Attard, H. Baltruschat, Quantitative DEMS study of ethanol oxidation: Effect of surface structure and Sn surface modification, Phys. Chem. Chem. Phys. 14 (2012) 16115–16129.

[27] H. Wang, Z. Jusys, R.J. Behm, Ethanol electro-oxidation on carbon-supported Pt, PtRu and Pt_3Sn catalysts: A quantitative DEMS study, J. Power Sources 154 (2006) 351–359.
[28] S. Pérez-Rodríguez, M. Corengia, G. García, C.F. Zinola, M.J. Lázaro, E. Pastor, Gas diffusion electrodes for methanol electrooxidation studied by a new DEMS configuration: Influence of the diffusion layer, Int. J. Hydrogen Energ 37 (2012) 7141–7151.
[29] J.P.I. De Souza, S.L. Queiroz, K. Bergamaski, E.R. Gonzalez, F.C. Nart, Electrooxidation of ethanol on Pt Rh, and PtRh electrodes. A study using DEMS and in-situ FTIR techniques, J. Phys. Chem. B 106 (2002) 9825–9830.
[30] H. Baltruschat, Differential electrochemical mass spectrometry, J. Am. Soc. Mass Spectrom. 15 (2004) 1693–1706.
[31] A.A. Abd-El-Latif, E. Mostafa, S. Huxter, G. Attard, H. Baltruschat, Electrooxidation of ethanol at polycrystalline and platinum stepped single crystals: A study by differential electrochemical mass spectrometry, Electrochim. Acta 55 (2010) 7951–7960.
[32] G.A. Camara, T. Iwasita, Parallel pathways of ethanol oxidation: The effect of ethanol concentration, J. Electroanal. Chem. 578 (2005) 315–321.
[33] S. Sun, M. ChojakHalseid, M. Heinen, Z. Jusys, R.J. Behm, Ethanol electrooxidation on a carbon-supported Pt catalyst at elevated temperature and pressure: A high-temperature/high-pressure DEMS study, J. Power Sources 190 (2009) 2–13.
[34] Y. Gao, H. Tsuji, H. Hattori, H. Kita, New on-line mass spectrometer system designed for platinum-single crystal electrode and electroreduction of acetylene, J. Electroanal. Chem. 372 (1994) 195–200.
[35] O. Guillén Villafuerte, G. García, J.L. Rodríguez, C. Arévalo, E. Pastor, New insight in the electrochemical oxidation of ethanol on carbon-supported Pt electrode by a novel electrochemical mass spectrometry configuration, Electrochem. Commun. 63 (2016) 48–51.
[36] M. Arenz, K.J.J. Mayrhofer, V. Stamenkovic, B.B. Blizanac, T. Tomoyuki, P.N. Ross, N.M. Markovic, The effect of the particle size on the kinetics of CO electrooxidation on high surface area Pt catalysts, J. Am. Chem. Soc. 127 (2005) 6819–6829.
[37] O. Guillén-Villafuerte, G. García, A. González Orive, B. Anula, A. Hernández-Creus, E. Pastor, Electrochemical characterization of 2D Pt nanoislands, Electrocatal. 2 (2011) 231–241.
[38] R. Gisbert, G. García, M.T.M. Koper, Oxidation of carbon monoxide on poly-oriented and single-crystalline platinumelectrodes over a wide range of pH, Electrochim. Acta 56 (2011) 2443–2449.
[39] S. Gilman, The mechanism of electrochemical oxidation of carbon monoxide and methanol on platinum. II. The 'reactant-pair mechanism for electrochemical oxidation of carbon monoxide and methanol, J. Phys. Chem. 68 (1964) 70–80.
[40] J.F. Gomes, K. Bergamaski, M.F.S. Pinto, P.B. Miranda, Reaction intermediates of ethanol electro-oxidation on platinum investigated by SFG spectroscopy, J. Catal. 302 (2013) 67–82.
[41] F. Colmati, E. Antolini, E.R. González, Ethanol oxidation on carbon supported Pt-Sn electrocatalysts prepared by reduction with formic acid, J Electrochem. Soc. 154 (2007) B39–B47.
[42] S. Rousseau, C. Coutanceau, C. Lamy, J.M. Léger, Direct ethanol fuel cell (DEFC): Electrical performances and reaction products distribution under operating conditions with different platinum-based anodes, J. Power Sources 158 (2006) 18–24.
[43] F. Vigier, C. Coutanceau, F. Hahn, E.M. Belgsir, C. Lamy, On the mechanism of ethanol electro-oxidation on Pt and PtSn catalysts: Electrochemical and in situ IR reflectance spectroscopy studies, J. Electroanal. Chem. 563 (2004) 81–89.
[44] E. Stenhagen, S. Abrahamsson, F.W. McLafferty (Eds.), Atlas of Mass Spectral Data, Interscience, New York, 1969.
[45] W. Chen, Q. Tao, J. Cai, Y.-X. Chen, The effect of alcohol concentration on the mass signal of CO_2 detected by differential mass spectrometry, Electrochem. Commun. 48 (2014) 10–12.
[46] E. Pastor, T. Iwasita, D/H exchange of ethanol at platinum electrodes, Electrochim. Acta 39 (1994) 547–551.
[47] J.L. Rodríguez, E. Pastor, X.H. Xia, T. Iwasita, Reaction intermediates of acetaldehyde oxidation on Pt(111) and Pt(100). An in situ FTIR study, Langmuir 16 (2000) 5479–5486.
[48] J. Silva-Chong, E. Mendez, J.L. Rodriguez, M.C. Arevalo, E. Pastor, Reactivity of acetaldehyde at platinum and rhodium in acidic media. A DEMS study, Electrochim. Acta 47 (2002) 1441–1449.
[49] J.A. Silva-Chong, O. Guillen-Villafuerte, J.L. Rodriguez, E. Pastor, DEMS study on the nature of acetaldehyde adsorbates at Pt and Pd by isotopic labeling, J. Solid State Electrochem. 12 (2008) 517–522.
[50] E. Mendez, J.L. Rodriguez, M.C. Arevalo, E. Pastor, Comparative study of ethanol and acetaldehyde reactivities on rhodium electrodes in acidic media, Langmuir 18 (2002) 763–772.
[51] G. García, J. Silva-Chong, J.L. Rodríguez, E. Pastor, Spectroscopic elucidation of reaction pathways of acetaldehyde on platinum and palladium in acidic media, J. Solid State Electrochem. 18 (2014) 1205–1213.
[52] J. Shin, W.J. Tornquist, C. Korzeniewski, C.S. Hoaglund, Elementary steps in the oxidation and dissociative chemisorption of ethanol on smooth and stepped surface planes of platinum electrodes, Surf. Sci. 364 (1996) 122–130.
[53] S. Fletcher, Tafel slopes from first principles, J. Solid State Electrochem. 13 (2009) 537–549.